

LASERS

PACS numbers: 42.55.Px; 42.60.Da; 42.60.Jf
DOI: 10.1070/QE2006v036n11ABEH013366

Simulation of emission characteristics and optimisation of waveguiding parameters of a ridge semiconductor heterolaser to maximise the emission brightness

S.A. Plisyuk, D.V. Batrak, A.E. Drakin, A.P. Bogatov

***Abstract*. The results of simulation of the emission characteristics of high-power ridge lasers at pump currents much higher than the threshold current are presented. The nonlinear interaction of carriers and the field in the laser cavity taking into account their distributions along the cavity axis and the influence of the inhomogeneous heating of the laser on the waveguiding effect are considered in the simulation. The dependence of the maximum single-mode output power on the ridge width W and the built-in step δn_b of the refractive index is studied. It is shown that a set of values of W and δn_b can be divided into four regions, each of which is characterised by its own type of the upset of lateral-single-mode operation. The calculated values of the threshold current, differential effici-ency and the far-field intensity distribution of laser emission agree well with the experiment.**

Keywords: *high-power ridge laser, lateral-single-mode operation, simulation of emission characteristics, emission brightness.*

1. Introduction

The problem of making of high-power semiconductor lasers is of current importance due to their wide application in open optical communication systems, information recording, the pumping of fiber lasers, etc. At present, several approaches to a semiconductor laser design exist, all of which yield comparable emission brightness, – these are the use of tapered waveguides [1], waveguides with a built-in slanted grating [2], and ridge waveguides [3]. In this paper, we consider the case of ridge waveguides. As noted in [3] and in references therein, the achievement of a bright stable radiation beam requires the optimisation of the geometrical parameters of a ridge waveguide, which determine the waveguiding effect in the horizontal direction (the waveguide in the plane of heterostructure layers). If the horizontal waveguide is weak, the anti-waveguiding effect of carriers, the influence of random stresses in the crystal and the temperature waveguide lead to the uncontrollable deformation of the output intensity distribution in the horizontal plane. If the horizontal waveguide is strong, a difference in gain between the first-order and zero-order lateral modes will be small, with the result that already at a small excess of the pump current over the threshold, a multi-lateral-mode operation accompanied by the change in the horizontal radiation pattern and the decrease of brightness will set in.

The technique for the optimisation of the geometrical parameters of ridge lasers described earlier [3] allows one to determine gain deficits for the lateral waveguide modes relative to the zero-order mode. However, the knowledge of the gain deficits does not yet allows us to answer the question about the maximum power attainable in a single-lateral-mode regime for a given ridge geometry. A further study of the possibilities for ridge geometry optimisation demanded the development of a ridge laser model which would consider the nonlinear interaction between the optical field and carriers in a laser cavity taking into account their distribution along the cavity axis. Furthermore, considering the influence of temperature distribution on the horizontal waveguiding effect is also required.

By now a number of papers exist, e.g. [4 – 9], which employ similar nonlinear models. But, as a rule, the calculations were carried out either for low-power lasers [6] or for gain-guided lasers [8]. As for high-power ridge lasers, operating in the output power range above 200 mW, their simulation remains of current interest. Meanwhile, it is just that level of power of single-lateral-mode ridge lasers which is especially demanded in modern applications. In view of the aforesaid, it was interesting to perform simulations of the emission characteristics of high-power ridge lasers and to compare the results with experimental data. This was the main goal of our study.

2. Calculation procedure

Simulation of the stationary emission characteristics of semiconductor ridge laser can be divided into two related problems. The first one is the calculation of a field distribution in the cavity with the given spatial dependence of the complex permittivity. The second one is the determination of the spatial distribution of the permittivity taking into account the inhomogeneous carrier distribution and the temperature profile in the cavity.

In semiconductor ridge lasers the field is linearly polarised and its lateral distribution is insensitive to the emission spectrum. This permits us to make a substantial simplification, considering only one monochromatic field component corresponding to one axial mode. Within the

S.A. Plisyuk, D.V. Batrak, A.E. Drakin, A.P. Bogatov P.N. Lebedev Physics Institute, Russian Academy of Sciences, Leninsky prosp. 53, 119991 Moscow, Russia; e-mail: bogatov@sci.lebedev.ru

Received 9 August 2006
Kvantovaya Elektronika **36** (11) 1058 – 1064 (2006)
Translated by D.V. Batrak

framework of the effective index approximation [3, 10], the field amplitude $E(\boldsymbol{r}, t)$ is sought in the form

$$E(x,y,z,t) = \mathrm{Re}\{v(x,y)[u^+(y,z)\exp(\mathrm{i}k_0 z) + u^-(y,z)\exp(-\mathrm{i}k_0 z)]\exp(-\mathrm{i}\omega t)\}, \quad (1)$$

where ω is the lasing frequency; k_0 is the wave number; $u^{\pm}(y,z)$ are the functions, characterising the field amplitude distribution in the plane of heterostructure layers (along Y axis); $v(x,y)$ is the field distribution in the plane perpendicular to the heterostructure layers (along X axis), normalised by the condition $\int |v(x,y)|^2 \mathrm{d}x = 1$.

In modern semiconductor lasers the function $v(x,y)$ is determined in most cases only by the geometry and material composition of heterostructure layers, so it remains constant under all laser operation conditions. The determination of this function is described in detail in [3].

The effective permittivity $\varepsilon_{\mathrm{eff}}(y,z)$, being the result of a certain 'averaging' of the permittivity along the vertical axis, can be written in the form:

$$\varepsilon_{\mathrm{eff}}(y,z) = n_0^2 + \delta\varepsilon_{\mathrm{b}}(y,z) + \delta\varepsilon_N(y,z) + \delta\varepsilon_T(y,z), \quad (2)$$

where n_0^2 is the constant real term, considerably larger than the modulus of all other terms; $\delta\varepsilon_{\mathrm{b}}$ is the complex term specifying the profile of the built-in horizontal waveguide, which is determined by the ridge geometry; $\delta\varepsilon_N$ is the complex term and $\delta\varepsilon_T$ is the real term determining the contributions of carriers and temperature, respectively.

The complex term $\delta\varepsilon_N$ is described by the expression:

$$\delta\varepsilon_N = 2n_{\mathrm{a}}\Gamma\Delta n(N) - \mathrm{i}\frac{c}{\omega}G(N)\Gamma, \quad (3)$$

where n_{a} is the refractive index and $G(N)$ is the material gain in the active region; N is the carrier concentration;

$$\Gamma = \sum_{i=1}^{m}\int_{x_i-d/2}^{x_i+d/2} |v(x,y)|^2 \mathrm{d}x$$

is the total optical confinement factor; x_i is the coordinate of the centre of the ith active region along X axis; d is the thickness of the active layer, which is assumed to be equal for all layers; and m is the number of active layers.

In our case, the typical cavity lengths L are much larger than the diffusion length λ_{D} and than the pump region width. On the other hand, λ_{D} is larger than the radiation wavelength in the medium, so one may reckon that the existence of diffusion along the cavity axis Z leads only to the smoothing of the modulation of carrier density N, caused by the interference of field distributions u^+ and u^-. Hence in every cross section $z = z_i$ the function $N(y, z_i)$ is determined by the distribution of the sum of intensities $|u^+|^2$ and $|u^-|^2$ in that cross section. Therefore, we will use the one-dimensional stationary diffusion equation as an equation for N

$$\frac{\lambda_{\mathrm{D}}^2}{\tau_{\mathrm{sp}}}\frac{\partial^2 N}{\partial y^2} = \frac{N}{\tau_{\mathrm{sp}}} - \frac{J(y)}{mde} + \frac{\mathrm{Im}(\delta\varepsilon_N)}{8\pi\hbar dm}\left(|u^+|^2 + |u^-|^2\right), \quad (4)$$

where τ_{sp} is the spontaneous recombination time; e is the electron charge; $\hbar$ is the Planck constant. The first term on the right side of Eqn (4) describes spontaneous transitions, the second term – carrier injection, the third term – stimulated transitions. When the heterostructure contains several active layers, we suppose that carrier concentrations $N(y,z)$ in all of them are equal.

We assume that the distribution of the injection current density along the Y axis is described by a step function:

$$J(y) = \begin{cases} J_0, & |y| \leqslant W/2, \\ 0, & |y| > W/2, \end{cases}$$

where W is the ridge width.

The temperature profile of the effective permittivity $\delta\varepsilon_T$ is determined by the expresion

$$\delta\varepsilon_T(y) = 2n_0\frac{\partial n}{\partial T}\int T(x,y)|v(x,y)|^2 \mathrm{d}x. \quad (5)$$

The distribution $T(x,y)$ is determined for a planar heterostructure with the heat conductivity coefficient χ_i, the width w_i and the distribution of heat sources power density f given for each layer, i.e. we neglect the presence of ridge while solving the heating problem. For the calculation of the temperature profile $T(x,y)$ a technique close to that described in [11] was employed. The waveguiding effect in the horizontal plane is mainly influenced by the heat sources localised under the ridge – a Joule heat in the heterostructure layers and a carrier thermalisation heat in the active layer. Their density is

$$f(x,y) = \begin{cases} J(y)\Delta V_{\mathrm{qd}}/(dm) \text{ (in the active layer)}, \\ [J(y)]^2\rho_i \text{ (in other layers)}, \end{cases}$$

where ρ_i is the resistivity of the ith passive heterostructure layer; ΔV_{qd} is the voltage characterising the carrier thermalisation in the active layer (quantum defect).

By setting $k_0 = \omega n_0/c$, substituting expression (1) into the two-dimensional wave equation and using a slowly varying amplitude approximation, we obtain for $u^{\pm}$

$$\frac{\partial u^{\pm}}{\partial z} = \mp\frac{1}{2ik_0}\left[\frac{\partial^2 u^{\pm}}{\partial y^2} + \frac{\omega^2}{c^2}(\delta\varepsilon_{\mathrm{b}} + \delta\varepsilon_N + \delta\varepsilon_T)u^{\pm}\right], \quad (6)$$

In addition to Eqn (6), we specify the boundary conditions for the field at laser mirrors:

$$u^+(y,0) = \sqrt{R_1}u^-(y,0), \qquad u^-(y,L) = \sqrt{R_{\mathrm{out}}}u^+(y,L), \quad (7)$$

where R_1 and R_{out} are the mirror intensity reflection coefficients.

The output power is determined by the expression

$$P = \frac{cn_0}{8\pi}(1 - R_{\mathrm{out}})\int |u^+(y,L)|^2 \mathrm{d}y. \quad (8)$$

Equations (6) and (4) with boundary conditions (7) constitute the system of coupled equations. The self-consistent stationary solution of this system was found by the iterative method analogous to the Fox–Li method and described in [2]. In the numerical implementation of the foregoing iterations, the propagation of the field was calculated by the fast Fourier transform beam propagation

method (FFT-BPM) [12]. The equation, which is nonlinear with respect to N, was solved by the iteration method, described in [2]. The coupling of the field equation and carrier density equation was performed after each step of the BPM, i.e. after each translation of field from the cross section $z = z_i$ to the cross section $z = z_{i+1}$ a new distribution $N(y, z_{i+1})$ was calculated. This method of calculation is analogous to the coupled solution method described in [13].

3. Simulation results

By using the model presented above, we calculated the emission characteristics of a ridge laser with a rectangular-shaped ridge and one active $In_{0.2}Ga_{0.8}As$ quantum well layer. The parameters used in the calculations are given in Table 1. Dependences of the gain $G(N)$ and the refractive index change $\Delta n(N)$ on the carrier density N for the active region were calculated in accordance with [14].

Table 1. Laser parameters used in calculations.

Parameter	Parameter value
Lasing wavelength $\lambda_0 = 2\pi c\,\omega^{-1}/\mu m$	0.98
Constant component of the effective refractive index n_0	3.45
Reflectivity of the highly reflecting mirror R_1	0.95
Reflectivity of the output mirror R_{out}	0.05
Optical confinement factor Γ	0.012
Spontaneous lifetime τ_{sp}/ns	2
Diffusion length $\lambda_D/\mu m$	1.5
Active region thickness $d/\mu m$	0.008

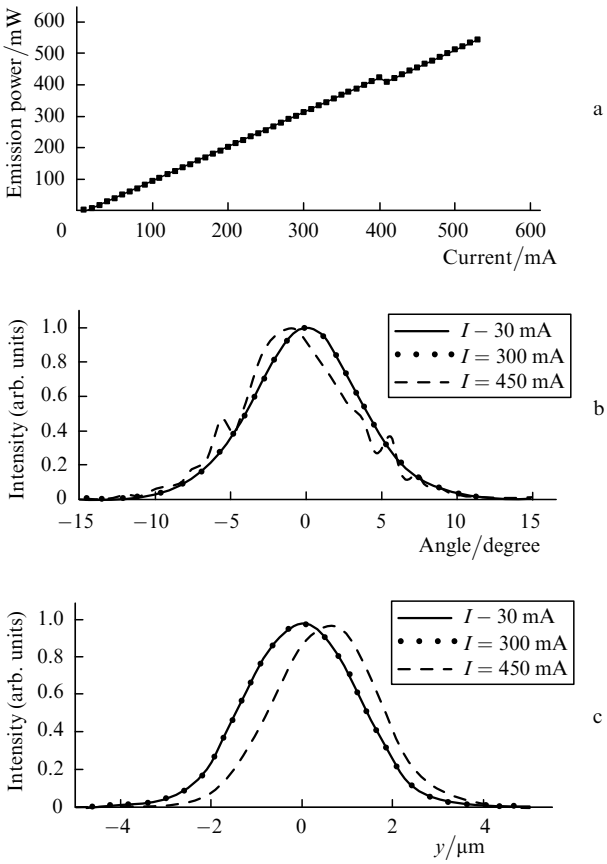

Figure 1. Calculated light–current characteristic (a) and far-field (b) and near-field (c) intensity distributions in the horizontal plane for a laser with $W = 4$ μm and $\delta n_b = 0.004$ at different values of I.

At first, for simplicity, we neglected the influence of a thermal waveguide. Figure 1 presents a typical calculated light–current characteristic and far-field and near-field intensity distributions in the horizontal plane for a laser with typical parameters – the ridge width $W = 4$ μm and the step of the effective refractive index produced by the ridge $\delta n_b = \mathrm{Re}(\delta\varepsilon_b)/(2n_0) = 0.004$. Figure 2 shows the distributions of the carrier density, the effective refractive index $n_{eff} = \mathrm{Re}\sqrt{\varepsilon_{eff}}$ and the effective gain near the highly reflecting mirror and near the output mirror of this laser at pump currents $I = 30$ and 300 mA (calculated threshold current $I_{th} = 15$ mA). One can see that already at $I/I_{th} = 2$, the maximum carrier densities near the highly reflecting mirror and near the output mirror differ by a factor of 1.7, and at $I/I_{th} = 20$ the shapes of carrier density distributions also differ appreciably, which leads to the difference in the distributions of $\delta\varepsilon$. One can see from Fig. 2c that at a pump current of 300 mA the gain for the zero-order mode near the highly reflecting mirror is more than twice larger than the gain near the output mirror. Therefore, nonlinear models of high-power lasers neglecting the distributions of carriers and field along the cavity axis are applicable only near the lasing threshold. For currents that are typical of the high-power ridge lasers, the distributions of N and $u^{\pm}$ along the cavity axis Z should be taken into account.

Apart from the power, the beam quality plays a great role in high-brightness lasers. In this connection, we investigated the dependence of the maximum output power, at which the field still remains single-mode, on the ridge width W and the built-in step of the refractive index δn_b. The studied set of parameters can be divided into four regions shown in Fig. 3. The first region is bounded by the value of the refractive index step comparable with the value of the anti-waveguiding contribution of carriers $\delta n_b \sim 0.001$. At such values of δn_b, whatever the value of W is taken, an initiation of lasing and output radiation characteristics are often determined not by the built-in horizontal waveguide, formed by the ridge geometry, but by the random contributions to the permittivity. All this leads to the change in the output characteristics from laser to laser which is often undesirable. Even if one assumes that all the uncontrollable variations of ε are eliminated, the influence of carriers will lead to the formation of gain-guiding in the laser, the far-field distribution will depend strongly on the pump current, and the M^2-factor for the output beam will become much more than unity. This is illustrated by the calculated light–current characteristic, far-field radiation patterns for two pump current values and corresponding M^2-factors presented in Fig. 4 for $W = 4$ μm and $\delta n_b = 0.001$.

The second region in Fig. 3 is the region of a relatively 'weak' waveguide. Its characteristic feature is that over the whole range of pump currents only a zero-order lateral mode exists. The calculated output power in this region is not limited (the calculation was performed up to the power of 1 W) for the parameters given in Table 1 and the zero-order mode profile is virtually constant over the whole range of pump currents. In practice the power of lasers with such parameters will be limited by the radiation flux density at which the optical breakdown of the output laser mirror takes place. For example for $W = 3$ μm and $\delta n_b = 0.005$ the optical flux density approaches the critical value

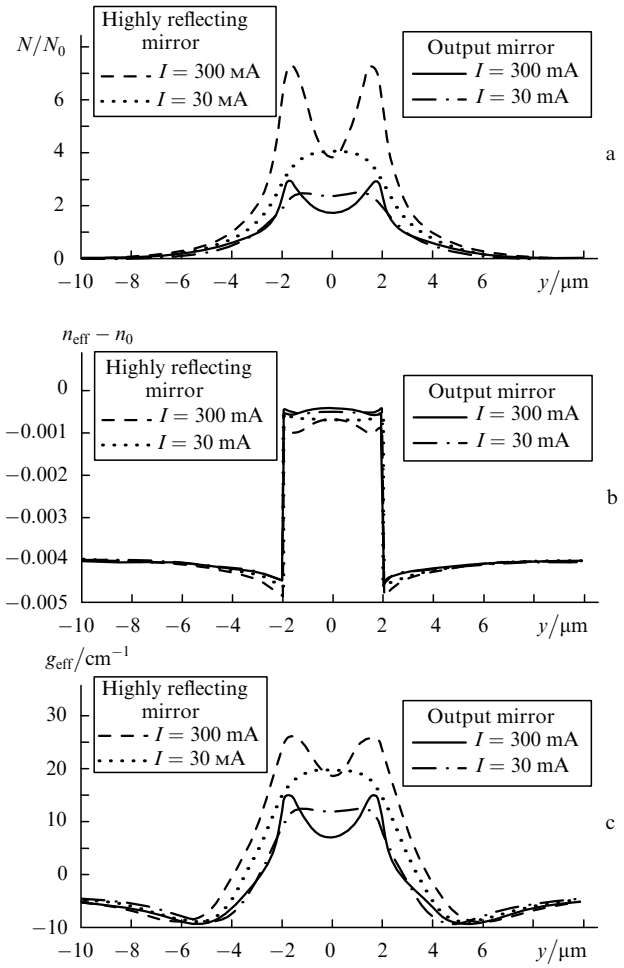

Figure 2. Distributions of the carrier concentration N (a), the effective refractive index n_{eff} (b) and the effective gain g_{eff} (c) near the highly reflecting and output laser mirrors at pump currents two times and twenty times larger than the threshold current ($I_{\text{th}} = 15$ mA) for a laser with $W = 4$ μm and $\delta n_{\text{b}} = 0.004$.

($\sim 2 \times 10^7$ W cm^{-2}) already at the output power of approximately 300 mW.

In region *4*, which is characterised by relatively large values of δn_{b} and W, the waveguide can support more than

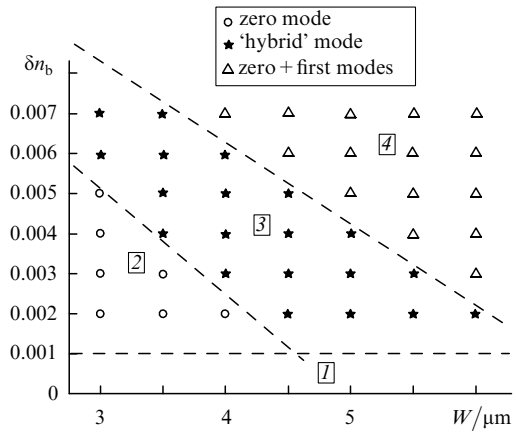

Figure 3. Regions of the ridge width W and the built-in refractive index step δn_{b} values with different types of single-lateral-mode generation upset (a separation by straight lines is conventional).

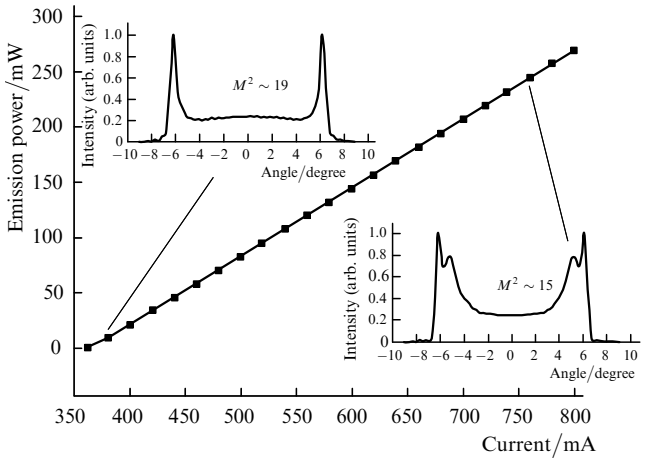

Figure 4. Calculated light–current characteristic, far-field intensity distributions in the horizontal plane, and M^2-factor values for a laser with $W = 4$ μm and $\delta n_{\text{b}} = 0.001$.

one mode ('strong' waveguide). Even at low pump levels the ratio of mode gains for the first- and zero-order lateral modes is close to unity. Therefore already at currents $I > (2-5)I_{\text{th}}$ a mode gain for the first-order mode reaches the threshold value. This limits the maximum single-mode output power at the level of 120 mW.

In region *3* – intermediate between regions *2* and *4* – the waveguide supports more than one mode too, but the ratio of mode gains for the first- and zero-order modes is appreciably less than unity. Thus for $W = 4$ μm and $\delta n_{\text{b}} = 0.004$ a mode gain for the first-order lateral mode, calculated within the linear approximation for the fixed $\varepsilon_{\text{eff}}(y, z)$ distribution, corresponding to the field distribution at the power near to the upset of the single-mode generation, is ~ 7 cm^{-1}, which is 8 cm^{-1} lower than the generation threshold. In this particular region the maximum single-mode output power is limited both by a beam steering effect [15–17] and by the optical breakdown. However, since W in this case can be somewhat larger than in region *2*, one can expect that the optical breakdown will occur at a larger output power. For the given values from Table 1, optimal geometrical ridge parameters are found in region *3*. Thus, for example, for $W = 4$ μm and $\delta n_{\text{b}} = 0.004$ the beam steering effect emerges at the power of 430 mW and the critical power flux $\sim 2 \times 10^7$ W cm^{-2} is reached at the power of 360 mW.

So it is just region *3*, along with region *2*, that can be considered as a region of the most optimal waveguide parameters in the view of obtaining a maximum radiation brightness.

The beam steering effect is most clearly illustrated in Fig. 5, showing the radiation intensity distribution in the laser cavity volume. A snake-like nature of beam propagation can be interpreted as an appearance of a nonlinear hybrid mode, being a certain superposition of zero- and first-order modes. A Fox–Li method does not allow us to discover all possible solutions in pure form. It only gives one self-consistent field distribution with the largest gain. Therefore, if the gain for the first-order mode is leveled up with the gain for the zero-order mode and, at the same time, a stationary generation is possible, then the solution will automatically take the form of such a hybrid mode. Obviously the resulting amplitude distribution at the output

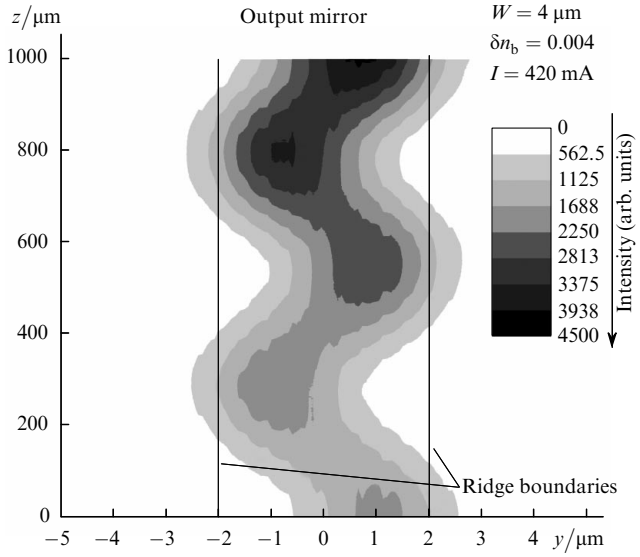

Figure 5. Distribution of the total field intensity $|u^+|^2 + |u^-|^2$ over the cavity of a laser with $W = 4$ μm and $\delta n_b = 0.004$.

mirror will depend on the phase relationships between the zero- and first-order modes, and so it is extremely sensitive to the values of working parameters (current, temperature etc.). This leads to the 'wandering' of the beam both in the near and in the far zones when the working parameters (e.g. pump current) change. Note that the phase relationships are by no means always such that they remain the same after the round trip of such a hybrid mode over the cavity. In that case Fox–Li iterations cease to converge, which means that no stationary solutions exist. An analogous but somewhat simpler interpretation of the beam steering effect as an emergence of a hybrid mode was proposed earlier in [15–17].

The consideration of the induced thermal waveguide does not change a qualitative division of the parameter set into the mentioned regions but deforms the boundaries between them. Figure 6 presents the simulation results for the laser with $W = 3$ μm and $\delta n_b = 0.004$ with and without taking the thermal waveguide into account. In the former case at the current of 500 mA a hybrid mode emerges and numerical iterations cease to converge. Thus, the thermal waveguide shifts a working point from region *2* to region *3* because the heating of the pump region leads to the growth and broadening of the n_{eff} profile (Fig. 6b).

Figure 7 presents the results of simulation and experimental study of the light–current characteristic and far-field intensity distributions in the horizontal and vertical planes for an AlGaAs/GaAs ridge laser emitting at 0.81 μm described in [18]. One can see from Fig. 7c that, as stated above, the measured intensity distribution in the vertical

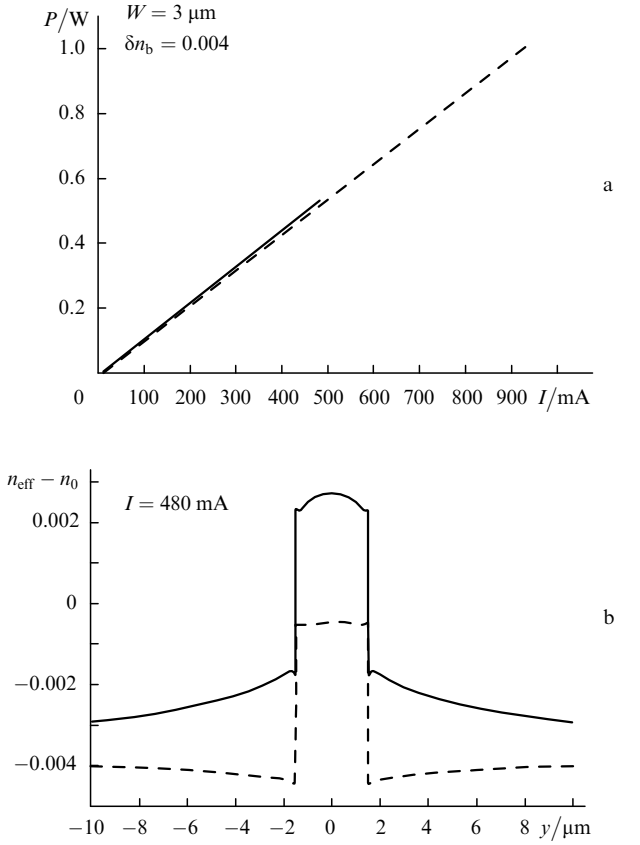

Figure 6. Comparison of calculated light–current characteristics (a) and distributions of the effective refractive index at the output mirror (b) taking (solid lines) and not taking (dashed lines) into account the thermal waveguide for a laser with $W = 3$ μm and $\delta n_b = 0.004$; $I = 480$ mA.

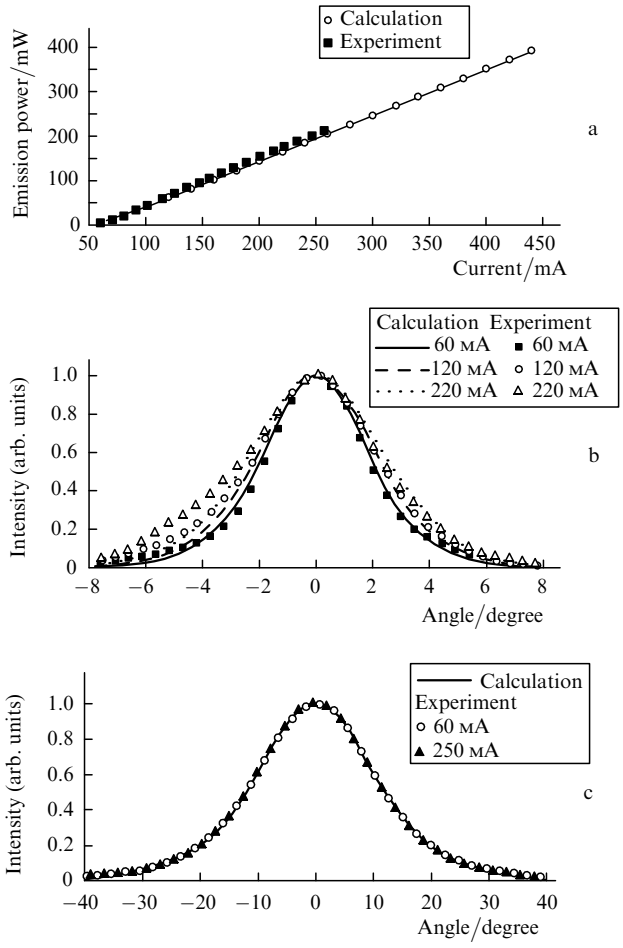

Figure 7. Comparison of the calculated characteristics (present work) and experimental radiative characteristics of a ridge AlGaAs/GaAs laser ([18]): light–current characteristics (a) and far-field intensity distributions in the horizontal (b) and vertical (c) planes.

direction is independent of the operating conditions of laser and coincides with the calculated distribution. The calculated threshold current and differential efficiency agree well with experimentally measured values (Fig. 7a). The calculated value of the maximum current, up to which single-mode operation persists, is 440 mA, but one can see from the experimental data (Fig. 7b), that at the current of 220 mA a horizontal far-field intensity distribution deforms and becomes asymmetrical. This means that in the experiment a beam steering effect appeared earlier than the simulation predicted. The reason for such a discrepancy could be the deviation of the real ridge shape from the computational one (for example, its changing along the cavity axis) or the quantitative difference between the calculation and real parameters, characterising an anti-waveguiding carrier effect.

4. Conclusions

The nonlinear model presented above for the interaction of optical field with carriers allows one to calculate numerically the radiative characteristics of ridge lasers taking into account the distributions of field and carriers along the cavity axis. These calculations, in contrast to the linear model [3], determining gain deficits for different lateral modes at the lasing threshold (for the fundamental mode), allow one to determine the optimal deficit value for a given heterostructure for the purpose of maximising single-lateral mode power.

The study of the maximum emitted power versus the ridge width W and the built-in step of the effective refractive index δn_b showed that, on the one hand, at small W, lying in region *2* (see Fig. 3), the field distribution remains single-lateral-mode up to the currents several tens of times larger than the threshold current, in the wide range of δn_b values. At larger ridge widths, lying in region *4*, a first-order mode emerges already at the currents only several times larger than the threshold value even for $\delta n_b = 0.002$. A minimum ridge width is determined by the optical breakdown of laser diode facets, while from above it is limited by the onset of multimode generation. At small δn_b a lasing regime is possible with the waveguide formed by gain and the emission characteristics may vary in a random way from one device to another. As to the large values of δn_b, a multi-mode generation occurs as well. Thus for each heterostructure, the optimal values of ridge width and refractive index step requiring a calculation exist at which a maximum brightness and a stable field distribution are achieved.

The consideration of the distributions of the field and carrier concentration along Z axis is important for high-power ridge lasers because the distributions of field and mode gains near the highly reflecting mirror and near the output mirror can differ significantly.

Note that the threshold current, the differential efficiency and the far-field intensity distributions at different pump currents, calculated in this work, well agree with the experimental results for the laser studied in [18].

The analysis of a variety of numerical results obtained for the emission characteristics of lasers at high ($\sim 10^7$ W cm^{-2}) optical flux density allows us to clarify the general qualitative picture of the self-action of optical flux propagating through the active region. Its physical nature is well known and is due to the spatial hole burning with the subsequent spatial variation of complex permittivity, i.e. the change in the gain and refractive index. Moreover, we can consider that the spatial variation of the refractive index manifests itself more dramatically than the gain variation. Nevertheless, separating the influence of the change in gain from the influence of the change in refractive index is hardly possible in pure form. They all are the manifestation of optical nonlinearity. In the borderline cases, e.g. for a strong enough waveguide ($\delta n_b \gg 3 \times 10^{-3}$), when the built-in refractive index step is larger than the change in refractive index due to hole burning, this optical nonlinearity leads mainly to the change in beam spatial profile through the excitation of modes with different lateral indices. In this case, one can suppose that the lateral amplitude distribution for each particular mode coincides with the distribution for the same mode at lasing threshold. In other words, in this case different lateral modes are 'mixed up' as a result of the optical nonlinearity, every mode being the solution of the linear problem.

Another borderline case can be distinguished too, when the waveguide is weak ($\delta n_b \gg 1 \times 10^{-3}$) or multi-mode ($W > 5$ μm). In this case, due to nonlinearity a spatial distribution can no longer be represented as a set of modes of any constant waveguide, it simply does not exist. For every laser power, there is a certain permittivity profile with a corresponding self-consistent lateral distribution of field amplitude. Staying in terms of modes, one might speak about a certain nonlinear mode which undergoes self-deformation when the laser output power (or the pump current) changes.

The nonlinear nature of the problem can lead to the multiple-valued dependence of output power on the pump current. Thus, it was shown that the thermal contribution to the horizontal waveguide can cause the deformation of boundaries between regions with different scenarios of lateral-single-mode generation upset. This can lead, in particular, to an increase in noise at random pulse modulation in a high-power operation regime. In this situation, when the pump current is modulated by a random sequence of pulses, the inhomogeneity of temperature distribution and, correspondingly, the thermal waveguide can depend on the past history of pump current changes before coming to the given working point, and so when working at maximum power the output power will also depend on the past history, which can lead to a drastic increase in noise during data transmission.

References

1. Walpole J.N. *Opt. Quantum Electron.*, **28**, 623 (1996).
2. Paschke K., Bogatov A.P., Drakin A.E., Güther R., Stratonnikov A.A., Wenzel H., Erbert G., Trankle G. *IEEE J. Sel. Top. Quantum Electron.*, **9** (3), 835 (2003).
3. Popovichev V.V., Davydova E.I., Marmalyuk A.A., Simakov A.V., Uspenskii M.B., Chel'nyi A.A., Bogatov A.P., Drakin A.E., Plisyuk S.A., Stratonnikov A.A. *Kvantovaya Electron.*, **32** (12), 1099 (2002) [*Quantum Electron.*, **32** (12), 1099 (2002)].
4. Agrawal G.P., Joyce W.B., Dixon R.W., Lax M. *App. Phys. Lett.*, **43** (1), 11 (1983).
5. Agrawal G.P. *J. Lightwave Technol.*, **2** (4), 537 (1984).
6. Witzigmann B., Witzig A., Fichtner W. *IEEE Transactions Electron Devices*, **47** (10), 1926 (2000).
7. Borruel L., Sujecki S., et al. *Proc. SPIE Int. Soc. Opt. Eng.*, **4646**, 355(2002).
8. Lim Jun Jun, Benson T.M., Larkins E.C. *IEEE J. Quantum Electron.*, **41** (4), 506 (2005).

9. Napartovich A.P., Elkin N.N., Sukharev A.G., Troshchieva V.N., Vysotsky D.V., Nesnidal M., Stiers E., Mawst J., Botez D. *IEEE J. Quantum Electron.*, **42** (6), 589 (2006).
10. Batrak D.V., Plisyuk S.A. *Kvantovaya Elektron.*, **36** (4), 349 (2006) [*Quantum Electron.*, **36** (4), 349 (2006)].
11. Menesguen Y., Kuszelewicz R. *IEEE J. Quantum Electron.*, **41** (7), 901 (2005).
12. Feit M.D., Fleck J.A. Jr. *Appl. Opt.*, **17** (24), 3990 (1978).
13. Wykes J.G., Borruel L., Sujecki S., Sewell P., Benson T.M., Larkins E.C., Esquivias I. *Proc. 4th Intern. Conf. on Computation Electromagnetics* (Bournemouth, UK, April 2002) p. 7.
14. Wenzel H., Erbert G., Enders P.M. *IEEE J. Sel. Top. Quantum Electron.*, **5** (3), 637 (1999).
15. Guthrie J. et al. *IEEE Phot. Tech. Lett.*, **6** (12), 1409 (1994).
16. Schemmann M.F.C. et al. *Appl. Phys. Lett.*, **66** (8), 920 (1995).
17. Herzog W.D., Goldberg B.B., Unlu M.S. *IEEE Phot. Tech. Lett.*, **12** (12), 1604 (2000).
18. Plisyuk S.A., Akimova I.V., Drakin A.E., Borodaenko A.V., Stratonnikov A.A., Popovichev V.V., Bogatov A.P. *Kvantovaya Elektron.*, **35** (6), 515 (2005) [*Quantum Electron.*, **35** (6), 515 (2005)].